3   # Metabolite profiling and peptidoglycan analysis of

4   # transient cell wall-deficient bacteria

5   # in a new *Escherichia coli* model system

6

7   Alexander Cambré[1, 2], Michael Zimmerman[3], Uwe Sauer[3], Bram Vivijs[2],

8   William Cenens[2], Chris W. Michiels[2], Abram Aertsen[2], Martin J. Loessner[4],

9   Jean-Paul Noben[5], Juan A. Ayala[6], Rob Lavigne[1], Yves Briers[1],*

10

11   [1] Laboratory of Gene Technology, Department Biosystems, KU Leuven, B-3001 Heverlee, Belgium

12   [2] Laboratory of Food Microbiology, Department of Microbial and Molecular Systems, KU Leuven, B-
13   3001 Heverlee, Belgium

14   [3] Institute of Molecular Systems Biology, ETH Zurich, CH-8093 Zurich, Switzerland

15   [4] Institute for Food, Nutrition and Health, ETH Zurich, CH-8092 Zurich, Switzerland

16   [5] Biomedical Research Institute, Hasselt University, B-3590 Diepenbeek, Belgium

17   [6] Centro de Biologia Molecular "Severo Ochoa", Campus de Cantoblanco, E-28049 Madrid, Spain

18

19   * Corresponding author

20   yves.briers@kuleuven.be

21   Kasteelpark Arenberg 21 bus 2462

22   B-3001 Leuven

23   Belgium

24   Tel. +32 16 379524

25   Fax. +32 16 321965

26

27

28   **Abstract**

29   Many bacteria are able to assume a transient cell wall-deficient (or L-form) state

30   under favorable osmotic conditions. Cell wall stress such as exposure to β-lactam antibiotics

31   can enforce the transition to and maintenance of this state. L-forms actively proliferate and

32   can return to the walled state upon removal of the inducing agent. We have adopted

33   *Escherichia coli* as a model system for the controlled transition to and reversion from the L-

34   form state, and have studied these dynamics with genetics, cell biology and 'omics'

35   technologies. As such, a transposon mutagenesis screen underscored the requirement for

36   the Rcs phosphorelay and colanic acid synthesis, while proteomics show only little

37   differences between rods and L-forms. In contrast, metabolome comparison reveals the high

38   abundance of lysophospholipids and phospholipids with unsaturated or cyclopropanized

39   fatty acids in *E. coli* L-forms. This increase of membrane lipids associated with increased

40   membrane fluidity may facilitate proliferation through bud formation. Visualization of the

41   residual peptidoglycan with a fluorescently labeled peptidoglycan binding protein indicates

42   *de novo* cell wall synthesis and a role for septal peptidoglycan synthesis during bud

43   constriction. The DD-carboxypeptidases PBP5 and PBP6 are three- and four-fold upregulated

44   in L-forms, indicating a specific role for regulation of crosslinking during L-form proliferation.

45

46

Introduction

48   Bacteria possess a multitude of mechanisms to survive under harmful conditions. A

49 well-known example is the formation of endospores as a response to nutrient depletion.

50 Endospores are able to resist extreme environmental stress, but can germinate when

51 favorable conditions are reestablished (Errington, 2003). Persister cells also remain viable in

52 spite of adverse long-term antibiotic exposure (Lewis, 2010). A metabolic shutdown makes

53 them insensitive to antibiotics. The discovery of persistence dates back over 60 years, but

54 yet only recently, their clinical significance is being readdressed, specifically in chronic

55 infections. First insights in the underlying molecular mechanisms have now become available

56 (Kester and Fortune, 2014). L-forms are another antibiotic-tolerant phenotype that is known

57 for many decades, but still remains cryptic, especially at the molecular level. Bacterial L-

58 forms result from the transition of normal, walled bacteria to a cell wall-deficient state. The

59 loss of an intact cell wall can be induced in several ways, e.g., exposure to cell wall-degrading

60 compounds such as lysozyme, to inhibitors of cell wall-synthesis such as β-lactam antibiotics,

61 but also through nutrient depletion (Allan *et al.*, 2009; Mearls *et al.*, 2012). As a

62 consequence, L-forms are often resistant to antibiotics that are active on the cell wall

63 (Domingue, 1982). Importantly, L-forms are viable and multiply by alternative reproduction

64 mechanisms such as external and internal budding, extrusion-resolution and (a)symmetrical

65 fission (Briers *et al.*, 2012a). L-forms are subdivided according to the extent of cell wall-

66 deficiency and their stability. Whereas spheroplasts have some residual peptidoglycan,

67 protoplasts completely lack any cell wall. Unstable L-forms can revert to the walled state

68 when they are no longer exposed to the inducer, whereas stable L-forms continuously

69 reproduce as such even in the absence of such an inducer (Allan *et al.*, 2009).

70   The clinical significance of L-forms is controversial and subject of much debate

71 (reviewed by Domingue and Woody, 1997; Mattman, 2001; Allan *et al.*, 2009). Whereas

72 some attribute virulent properties to L-form, the hypothesis that unstable L-forms may be an

73 escape route in response to cell wall stress has more support. Recurrent transitions and

74 reversions between walled and unwalled cellular states may contribute to relapsing bacterial

75 infections. In this view, virulence and pathogenicity is only associated with the walled state,

76 whereas the cell wall-deficient state is responsible for prolonged persistence in the human

77 body. Other authors dispute any clinical role for L-forms (Onwuamaegbu *et al.*, 2005; Lantos

78 *et al.*, 2014; Schnell et al., 2014). They emphasize the lack of uniformity of techniques used

79 to identify L-forms and argue that current evidence for their clinical significance is mainly

80 based on case reports. Generally, all contributors agree more studies are needed to clarify

81 the clinical significance of L-forms (Allan *et al.*, 2009). However, research on cell wall-

82 deficiency is challenging due to the fastidious character of L-forms and their pleomorphic

83 nature. There has been a lack of genetically tractable L-form model systems that can be

84 produced under standardized and reproducible conditions. Recently, important progress was

85 made with the introduction of a *Bacillus subtilis* (Leaver *et al.*, 2009; Dominguez-Cuevas *et*

86 *al.*, 2012; Mercier *et al.*, 2012) and a *Listeria monocytogenes* (Dell'Era *et al.*, 2009; Briers *et*

87 *al.*, 2012b) L-form model system. However, both models are stable L-forms that do not

88 revert when the inducer is removed (except by genetic restoration of cell wall synthesis;

89 Kawai *et al.*, 2014) . Ranjit and Young (2013) described lysozyme-induced *E. coli* spheroplasts

90 that spontaneously recover a rod shape, however, it has not been reported whether these

91 spheroplasts can replicate autonomously in the presence of the inducing factor.

92   We present here a reversible model of transient cell wall-deficiency based on

93 *Escherichia coli* MG1655, in which all cells quantitatively undergo transition and reversion.

4

94   Therefore, this model allows to study transition, L-form reproduction and reversion in a

95   controlled manner within a single model. Using this model, we show that in spite of limited

96   differences at the proteome level, the L-form metabolome is featured by a high abundance

97   of (lyso)phospholipids that increase membrane fluidity. A residual amount of peptidoglycan

98   precursors and peptidoglycan turnover products is detected in actively multiplying L-forms.

99   We show the location of the low amount of newly synthesized peptidoglycan during L-form

100   reproduction, and visualize the resumption of the full peptidoglycan synthetic capacity

101   during reversion to rods.

102

103   **Results**

104   *Visualization and quantification of transition, L-form growth and reversion*

105   An ideal *in vitro* L-form model system should meet several requirements: (1) the

106   transition and reversion should be quick, quantifiable and at will, (2) to enable easy

107   collection for analyses by demanding molecular techniques, the L-forms should be able to

108   grow in liquid media and finally, (3) their growth rate should not be too slow and they should

109   grow as colonies on a plate. The L-form model system described here meets all these

110   prerequisites and is based on *E. coli* L-forms described by Joseleau-Petit *et al.* (2007). *E. coli*

111   MG1655 – one of the most tractable organisms for molecular research – is induced to the

112   cell wall-deficient state in hypertonic M broth supplemented with 45 μg/ml β-lactam

113   cefsulodin (MCef45). In this liquid medium supplemented with cefsulodin they are able to

114   propagate in the absence of an organized cell wall and can easily revert to rods upon

115   antibiotic removal (Figure 1). The model describes thus unstable L-forms that can revert.

5

116   Transitions mostly occur at the septum or at the poles, and occasionally at other

117   positions along the cell wall, and invariably result in dumping an empty sacculus (Movie S1).

118   Successful transition results in actively reproducing L-forms in 25-50% of the cases, whereas

119   failed transitions result in prompt lysis. The transition rate has been quantified every 30

120   minutes after addition of cefsulodin. Transitions do not take place synchronously. Instead,

121   most L-forms escape from the sacculus between 60 and 300 minutes after cefsulodin

122   exposure. A transient subpopulation of transition intermediates that remain attached to the

123   sacculus, increases and decreases again as the balance between the rate of initial protoplast

124   escape and the formation of completely formed L-forms shifts (Figure 2A).

125   Once transition is completed, the suspension only contains L-forms that multiply

126   infinitely in the absence of an intact cell wall, as long as cefsulodin was present in the

127   medium. The reproduction trajectory differs depending on the culture conditions. In a liquid,

128   shaking culture with cefsulodin, L-forms multiply through the formation of relatively small

129   buds that are split off, possibly due to shear forces. On an agar pad with cefsulodin, initial

130   doublings of L-form cells often appear to be rather symmetrical (binary fission-like), whereas

131   later divisions become more asymmetrical with multiple, simultaneous membrane blebbing

132   events occurring in a single L-form. As a result, many pleiomorphic cells are formed. Tubular

133   protrusions that are eventually split off can also be observed (Movie S2). Growth rate in the

134   mid-exponential phase of L-forms (MCef45 broth) is lower (μ = 0.16 h^{-1}) than the growth rate

135   of rods in hypertonic medium without cefsulodin (M broth) (μ = 0.48 h^{-1}) or in reference LB

136   broth (μ = 0.56 h^{-1}). In addition, the maximal density of L-forms in the stationary phase is

137   about one third lower than the density of rods in the same hypertonic medium. Continuous,

138   spontaneous lysis of a fraction of the cells during proliferation will certainly contribute to a

139   reduced maximal density that can be achieved.

6

140   In liquid culture, reversion starts with filamentous outgrowths from the L-form

141   surface, which are eventually pinched off. On an agar pad, pleomorphic cells deform to a

142   more elongated shape, followed by outwards, filamentous growth at ectopic poles, leading

143   to branched cells (Movie S3). Already 30 minutes after cefsulodin removal, approximately

144   50% of the population shows such intermediate cell shapes, indicating a quick reversion, and

145   the proportion of L-forms gradually drops in the next 4.5 h. An almost isomorphic population

146   of rods appears after 5 hours (Figure 2B).

147   Altogether, this model system of *E. coli* MG1655 L-forms induced with cefsulodin

148   provides a good framework to study transition, L-form reproduction and reversion *in vitro*.

149

150

151   *Transposon mutagenesis underscores the necessity of the Rcs phosphorelay and*

152   *colanic acid synthesis for L-form survival*

153   A total of 5,760 mutants from a random transposon library were screened by replica

154   plating on both M and MCef45 agar for the capacity to undergo transition and multiply as L-

155   form cells. Fourteen transposon mutants in nine different genes could be identified as

156   growing on M agar but not on MCef45 agar (Table 1). Seven mutants are defective in the

157   colanic acid biosynthesis cluster (*wzc*, *wcaD, wcaE, wcaK,* and *wcaL*), two others in the

158   synthesis of colanic acid precursors (*galE*, *ugd*) and five more in the Rcs two-component

159   system (*rcsC, rcsD*). The latter system is activated by cell wall stress and regulates up to 150

160   genes, including genes involved in colanic acid synthesis. All mutants could be confirmed by

161   plating the corresponding single-gene, in-frame deletion mutants from the KEIO collection

162   (Baba *et al.*, 2006).

163   We used an MG1655 strain equipped with a chromosomal *rprA-lacZ* fusion to confirm

164   Rcs activation in L-forms (Majdalani *et al.*, 2002). The strain was grown either as regular rods

165   (in LB or hypertonic M broth) or as L-forms in (MCef45 broth), and β-galactosidase activity

166   was measured with o-nitrophenyl-β-D-galactoside. In hypertonic M broth, a two-fold

167   upregulation takes place, followed by a further 75-fold increase in MCef45. These data

168   clearly confirm the activation of the Rcs phosphorelay in L-forms (Figure S1).

169   Two other mutants were resistant to 45 µg/ml cefsulodin because they grew as rods

170   on MCef45 agar plates (which can be easily differentiated from L-form colonies due to a less

171   mucoid appearance). These mutants have a transposon insertion in *hrpB*, encoding a DNA

172   helicase. This gene is located directly upstream of *mrcB* that codes for PBP1B, the target of

173   cefsulodin. Upregulation of transcription of *mrcB* by an internal promoter of the transposon

174   has most likely outperformed the effect of cefsulodin. Consistently, the in-frame *hprB*

175   deletion mutant from the KEIO collection (Baba *et al.*, 2006), which misses this internal

176   promoter, grows as normal L-form colonies on MCef45 agar plates, excluding any essential

177   role of HrpB for L-form growth. In conclusion, (activation of) colanic acid synthesis is of

178   crucial importance for L-form growth.

179

180   *The L-form proteome is highly similar to the proteome of normal rods*

181   A comparison of the proteome of *E. coli* MG1655 rods grown in LB or M broth, and L-

182   forms in MCef45 broth was performed through 2D-PAGE and mass spectrometric analysis.

8

183   The proteome of L-forms surprisingly appears to be more identical to the proteome of rods

184   grown in LB (92.1%) than in M broth (86.8%) (n=419). There were no unique or strongly

185   overabundant protein spots present in the L-form samples. In contrast, 32 spots present

186   either in LB, M or both conditions were absent or less abundant in L-forms (Figure 3). These

187   proteins belong to diverse functional categories (Table S1). Two isoforms of isocitrate lyase

188   are absent under hypertonic conditions with and without cefsulodin, whereas a third

189   isoform is present but strongly less abundant (<10%) under these conditions. Isocitrate lyase

190   catalyzes the first step in the glyoxylate shunt in the TCA cycle, suggesting the glyoxylate

191   shunt is less active under hypertonic conditions. The inhibitor of vertebrate lysozyme (Ivy) is

192   only detected in M broth. It has been reported that the expression of Ivy is activated by the

193   two-component Rcs system that is triggered by cell wall stress (Callewaert *et al.*, 2009).

194   Although the Rcs system is also strongly activated in L-forms (Figure S1), Ivy appears to be

195   absent in the latter. Possibly periplasmic Ivy may be lost in the absence of an intact cell wall.

196   Two isoforms of the outer membrane protein A (OmpA) are detected in L-forms. Their

197   presence indicates that L-forms should have at least a rudimentary outer membrane,

198   although the exact nature and structure of the outer membrane of L-forms remains

199   unknown. Altogether, changes in the proteome of L-forms were found to be only limited.

200

201   *L-forms have an increased number of (lyso)phospholipids with unsaturated or*

202   *cyclopropanized fatty acid chains*

203   The large differences in morphology, life style and reproduction mechanism of L-form

204   argue for a different metabolism in spite of the largely conserved proteome. The

205   metabolome is the downstream outcome of the transcriptome and proteome and is

9

206   therefore closely associated with the physiology of a certain phenotype of the cell (Putri *et*

207   *al.*, 2013). To obtain an accurate snapshot of the actual physiological differences between

208   rods and L-forms, we compared the metabolome of rods grown in both reference broth (LB)

209   and hypertonic broth (M), and of L-forms grown in hypertonic broth with cefsulodin

210   (MCef45). Rods grown in LB and exposed to cefsulodin lysed quickly, making sampling

211   impossible. Among three conditions tested, 310 different ions were assigned to 467 putative

212   metabolites (including mass isomers) from a total of 884 molecules contained in a genome

213   scale metabolic model of *E. coli* (Table S2) (Feist *et al.*, 2007; Fuhrer *et al.*, 2011). A wide

214   variety of metabolite classes were covered: carbohydrates, lipids, nucleotides, amino acids,

215   vitamins, cofactors, energy metabolism, terpenoids, polyketides and glycans. About half of

216   the detected metabolites (n=154) had a significantly different concentration under at least

217   one of the conditions ($\log_2(\mathrm{met}_i(\text{condition X})/\mathrm{met}_i(\text{condition Y}))>0.5$; $P<0.01$) (Table S2). The

218   differences in metabolite concentration were used to perform hierarchical clustering. Both

219   biological and technical replicates of each condition were grouped together, confirming the

220   reproducibility of each metabolic profile (Figure S2). A principal component analysis allowed

221   the identification of the most prominent metabolites that explain the majority of variance

222   between the different conditions (Figure S3). The first two components explain 94.6 % of

223   total variance, and were retained for analysis. The first component representing 85.3% of

224   the variance separates the metabolic profile of L-forms (MCef45) from those of rods (LB and

225   M) and has high component loadings for (cyclopropanized) phospholipids and

226   lysophospholipids. The second component (9.3%) mainly distinguishes the samples from

227   rods grown in hypertonic broth from the other conditions and is characterized by a high

228   component loading for reduced glutathione (Table S3). These results show that the three

229   conditions are mainly differentiated by their differences in (lyso)phospholipid metabolism

230   and the antioxidant glutathione.

231   In absolute terms, there is a clear increase of the total abundance of phospholipids in

232   L-forms (+65%/+46%, compared to LB and M, respectively) with cyclopropanized fatty acids

233   (+107%/+62%) and unsaturated acyl chains (+39%/+35%) responsible for the most

234   prominent changes, whereas the number of phospholipids with saturated fatty acids are

235   only slightly increased (+18%/+1%). Specifically, four out of fourteen detected phospholipids

236   have a significantly increased concentration in L-forms ($\log_2 > 0.5$; $P < 0.01$), specifically

237   phosphatidyl ethanolamine (16:1) ($\log_2$-fold increases of +0.42/+0.74) and its

238   cyclopropanized form (+1.14/+0.81), phosphatidyl ethanolamine (18:1) (+0.94/+0.58) and

239   cyclopropane phosphatidylglycerol (16:0) (+0.96/+0.52) (Figure 4). Peak heights of the ten

240   other, generally less abundant phospholipids are less different among the three conditions

241   (Table S2). Lysophospholipids or mono-acyl phospholipids show even more drastic changes

242   in the L-form metabolome (+385%/+531%, compared to LB and M, respectively). Especially

243   lysophospholipids with an ethanolamine headgroup and longer acyl chains (18:1; 16:1 and

244   16:0; +3.05/+3.16, +4.62/+4.38 and +4.18/+4.23 $\log_2$-fold changes, respectively) have a

245   higher concentration in L-forms. In contrast, lysophospholipids with a glycerol headgroup

246   and shorter acyl chains (12:0 and 14:1) are underrepresented in L-forms (-1.13/-0.26 and -

247   2.09/-0.91, respectively) (Figure 4). In conclusion, not only the total number of

248   (lyso)phospholipids is significantly higher in L-forms, but also the relative proportion of

249   phospholipids with unsaturated and cyclopropanized fatty acid chains has increased.

250   The decreased level of reduced glutathione in L-forms compared to rods grown in LB

251   and M (-2.26 and -4.09, respectively) may indicate an increased level of oxidative stress in

11

252   the cell wall-state. Reduced glutathione is one of the strongest bacterial antioxidants and

253   constitutes 99.5% of the total cellular amount of glutathione under unstressed conditions

254   (Smirnova and Oktyabrsky, 2005). Oxidative stress would result in an increase of oxidized

255   glutathione at the expense of the reduced form. However, oxidized glutathione was not

256   detected. An alternative explanation for the decreased level of reduced glutathione could be

257   that the total pool of glutathione is reduced in L-forms. Slightly decreased levels of

258   glutathione have been previously reported in slow-growing bacteria, and also the L-forms

259   analyzed here have a slower growth rate ($\mu = 0.16$ h^{-1} versus 0.48 and 0.56 h^{-1} for rods grown

260   in hypertonic and LB broth, respectively). This is possibly linked to the lower amount of

261   glutamate (-1.86/-1.10), which is required for glutathione synthesis (Tweeddale *et al.*, 1998).

262

263   *The residual amount of newly synthesized peptidoglycan collocates with buds and*

264   *constriction sites during L-form reproduction*

265   Different metabolites related to peptidoglycan synthesis (N-acetyl-muramine acid,

266   UDP-N-acetylmuramoyl-L-alanine, UDP-N-acetyl-glucosamine, meso-diaminopimelic acid (m-

267   DAP)) and to peptidoglycan turnover and recycling ((N-acetyl-D-glucosamine)-1,6-

268   anhydrous-N-acetylmuramyl-tetrapeptide, (N-acetyl-D-glucosamine)-1,6-anhydrous-N-

269   acetylmuramyl-tripeptide, L-alanine-D-glutamate-m-DAP, L-alanine-D-glutamate-m-DAP-D-

270   alanine) are detected in L-forms (Table S2). Although mostly in a lower abundance compared

271   to rods, their presence suggests active peptidoglycan synthesis and degradation. This is

272   consistent with the finding that residual peptidoglycan in cefsulodin-induced L-forms

273   accounts for 7% of the normal amount in rods and that its synthesis is essential for growth

274   and probably required for cell division (Joseleau-Petit *et al.*, 2007). To locate peptidoglycan

12

275 (residues) during transition, growth and reversion, we used a fusion protein that combines a

276 peptidoglycan binding domain (PBD) derived from the endolysin of bacteriophage φKZ and

277 GFP (PBD-KZ-GFP) (Briers *et al.*, 2007). Similar as observed for rods, addition of purified PBD-

278 KZ-GFP did not bind to the L-forms, indicating the presence of an effectively shielding outer

279 membrane in L-forms as in rods. Only after permeabilization of the outer membrane, the

280 peptidoglycan layer of rods is accessible for the fluorescent peptidoglycan binding protein

281 (Briers *et al.*, 2007). We used chemical fixation and permeabilization to remove the outer

282 membrane barrier. Fixation is needed to stabilize the osmotically unstable L-forms,

283 preventing lysis during permeabilization of the outer and inner membrane of the cells. After

284 fixation and permeabilization of the cells, we labeled cells with purified PBD-KZ-GFP at

285 different stages between the rod- and cell wall-deficient state (Figure 5).

286 During transition, the cell wall breaks open at the septum or the pole and the

287 cytoplasm is released as a protoplast, apparently completely devoid of peptidoglycan

288 remnants. A relatively intact sacculus is left behind. In contrast, growing and multiplying L-

289 forms show clear local accumulations of peptidoglycan, colocating with protruding buds. The

290 peptidoglycan does not sharply delineate the cell border as observed in rods, but is more

291 blurred. In general, the fluorescence intensity appears to increase with the bud size, but

292 remains lower than that of an intact sacculus in rods. During constriction of the buds,

293 peptidoglycan mostly locates at the constriction site. When cefsulodin is removed and

294 reversion starts, a strong fluorescence surrounds the protrusions, often expanding over the

295 spherical surface of the L-forms, or along the deformed, elongated shape of the reverting L-

296 form.

297

13

298   *L-forms have an increased level of DD-carboxypeptidases PBP5 and PBP6*

299   The complete loss of the sacculus during transition and the apparent absence of any

300   peptidoglycan suggest *de novo* peptidoglycan synthesis in L-forms. Penicillin-binding proteins

301   (PBPs) are required for the final steps of peptidoglycan synthesis, specifically for

302   polymerization of the precursors (transglycosylation) and cross-linking of adjacent chains

303   (transpeptidation). To quantify changes in the PBP profiles during conversion from the rod to

304   the cell wall-deficient state and back, we used Bocillin FL, a fluorescent penicillin, as a

305   labeling reagent for PBPs (Table 2) (Zhao *et al.*, 1999). A reference PBP profile of *E. coli*

306   MG1655 rods has been used for identification of the different identified PBPs (Figure S5).

307   Most prominent changes in the PBP profile were a three- and four-fold upregulation of PBP5

308   and PBP6 in L-forms in comparison to rods, respectively. PBP5 and PBP6 are two out of four

309   DD-carboxypeptidases encoded by *E. coli*, cleaving the terminal D-alanine from the

310   pentapeptide. Therefore, one would expect more terminal D-Ala residues to be removed

311   from peptidoglycan. This would in turn reduce the degree of cross-linking by transpeptidases

312   PBP1A and PBP1B (Templin *et al.*, 1999; Hesek *et al.*, 2004), influencing the cell shape.

313   Previously, it has been reported that elevated levels of PBP5 result in osmotically stable

314   spherical *E. coli* cells (Markiewicz *et al.*, 1982). The lack of terminal D-Ala residues may also

315   explain why approximately a doubling of DAP-DAP cross-links were detected in *E. coli* L-

316   forms at the expense of DAP-D-Ala cross-links (Joseleau-Petit *et al.*, 2007). Interestingly,

317   lysozyme-induced *E. coli* spheroplasts lacking PBP5 or PBP6 show a delayed and altered

318   reversion to the rod shape (Ranjit and Young, 2013), further suggesting a modulating role for

319   these enzymes and the degree of cross-linking in the cell wall-deficient state.

320   Bifunctional transglycosylase/transpeptidases PBP1A and PBP1B are detected at

321   lower levels in samples from cells undergoing transition and L-forms. However, this

322   observation could be biased significantly by the acylation of these PBPs by the L-form

323   inducing agent cefsulodin, converting those PBPs to an unsuitable binding target of Bocillin

324   FL. Indeed, it has previously been shown that the transglycosylase moiety of PBP1B is

325   necessary for L-form growth, making the absence of PBP1B in L-forms unlikely (Joseleau-

326   Petit *et al.*, 2007). Extensive washing of the samples did not change this outcome, indicating

327   an extremely low deacylation rate of the PBP-cefsulodin complex.

328

329   **Discussion**

330   Bacteria encounter many adverse conditions in their natural life. It was quickly

331   understood that L-forms may be a possible escape route upon exposure to cell wall-

332   inhibiting antibiotics, immune serum, complement and bacteriophages and return to the

333   walled state when the inducing factor is removed (Dienes and Weinberger, 1951). Decades

334   of research on the phenomenon of cell wall-deficiency and survival as L-forms followed and

335   yielded a multitude of induction protocols and descriptions of their morphology,

336   reproduction mechanisms and cytological properties. However, knowledge of the molecular

337   cell biology of (transient) cell wall-deficiency is still in its infancy. First, because the research

338   field peaked before the introduction of modern molecular tools in microbiology, and second,

339   because of the lack of tractable model systems to study transition, growth and reversion.

340   Expanding from *E. coli* L-forms described by Joseleau-Petit *et al.* (2007), we here describe a

341   model of transient cell wall-deficiency. The three steps in a cycle of transient cell wall-

342   deficiency (transition, L-form reproduction and reversion) can be fully controlled and

15

343   visualized. This allows to study transition, L-form reproduction and reversion both at the

344   population level (using omics technologies) and at the single cell level (using fluorescence

345   microscopy). An important feature is the quantifiable nature of the model. Induced L-forms

346   and reverting L-forms grow on a plate and can be quantified as single colonies that grow

347   from a single cell, which is in contrast to most other L-form systems that do not grow on agar

348   plates. This allows to study quantitative effects of different growth conditions or mutants.

349   Transition takes place at the septum and recently formed cell poles, but only rarely

350   along the lateral cell wall, which is mostly the case in *B. subtilis* L-forms (Domínguez-Cuevas

351   *et al.*, 2012). Cefsulodin inhibits the transpeptidase activity of the bifunctional penicillin-

352   binding proteins PBP1A and PBP1B, the major enzymes for peptidoglycan synthesis in *E. coli*.

353   PBP1B is located both at the septum, poles and lateral cell wall (Bertsche *et al.*, 2006), but it

354   may not be surprising that a cell wall defect – large enough for protoplast escape – most

355   easily occurs at the septal site.

356   Whereas division follows a relatively uniform path in *E. coli* rods, division in L-forms

357   ranges from binary fission-like division, asymmetrical fission to the formation of small buds.

358   Especially on agar pads, aberrant and extremely pleomorphic cells can be formed. This is

359   consistent with our previous hypothesis that L-forms have a proliferative mechanism that is

360   typically less efficient, less coordinated, and slower (Briers *et al.*, 2012a). Although the L-

361   form genome encodes all elements for a functional divisome and elongasome, the structural

362   organization and tight links between both machineries are lost. In this perspective, it has

363   been found previously that MreB becomes dispensable, while FtsZ remains essential for

364   viability of cefsulodin-induced *E. coli* L-forms (Joseleau-Petit *et al.*, 2007).

16

365   All observed genetic requirements necessary for L-form growth and multiplication

366   can be attributed to the formation of the capsular polysaccharide colanic acid. The Rcs two-

367   component sensor kinase system, genes involved in precursor synthesis and synthesis of the

368   colanic acid polymer were identified. The presence of colanic acid was already obvious from

369   the mucoid appeareance of *E. coli* L-form colonies, and its requirement was confirmed

370   previously for cefsulodin- and penicillin-induced *E. coli* L-forms (Joseleau-Petit *et al.*, 2007;

371   Glover *et al.*, 2009). Considering the finite number of transposon mutants, the existence of

372   other essential genes for L-form growth cannot be excluded. However, because of the

373   randomness of the library (approximately 1% of the mutants are confirmed to be auxotroph,

374   corresponding to the theoretical proportion) and multiple independent hits in the same

375   genes, it is unlikely that other large clusters of related genes could be identified.

376   Especially in view of the drastic changes of the phenotype of L-forms, the proteome

377   of L-forms shows remarkably high similarity to the wildtype proteome. No single additional

378   or significantly upregulated proteins were identified in the 2D map of the L-form proteome.

379   However, when the metabolome was compared, large changes were observed with half of

380   the detected ions having a significantly different concentration (154/310; $\log_2 > 0.5$; $P < 0.01$).

381   This indicates that most of the changes take place at the level of the metabolism through

382   differences in enzyme activity, in allosteric regulation of enzymes and in fluxes through

383   metabolic pathways.

384   There is an obvious shift of C-atoms from carbohydrates, amino acids and nucleotides

385   to (lyso)phospholipids. The higher total amount of phosphoslipids in L-forms may be

386   surprising, since the transition from rod to sphere is accompanied by a decrease in the

387   surface/volume ratio, which would suggest a lower need for phospholipids. However,

17

388   Bendezú and De Boer (2008) have previously shown that spherical *E. coli mreB* mutants are

389   unable to adjust their phospholipid synthesis rate to changes in the surface area, resulting in

390   a membrane excess. The increased proportion of phospholipids observed in *E. coli* L-forms

391   also further supports the hypothesis that L-form reproduction generally depends on

392   biophysical membrane dynamics driven by the imbalance between cell membrane and

393   volume (Briers *et al.*, 2012a; Leaver *et al.*, 2009; Mercier *et al.*, 2013).

394   Membrane fluidity is a key factor that allows membrane deformations to effectively

395   result in new progeny. In *Bacillus subtilis* L-forms, sufficient membrane fluidity is achieved

396   through the synthesis of branched chain fatty acids (Mercier *et al.*, 2013). *E. coli* produces

397   only straight-chain fatty acids, but likely achieves the same outcome with an increased level

398   of phospholipids having unsaturated and cyclopropanized acyl chains (Figure 4, Table S2).

399   Indeed, both unsaturated and cyclopropanized fatty acids have a poor acyl chain packing

400   capacity in the phospholipid bilayer (Perly *et al.*, 1985). Cyclopropanized phospholipids result

401   from the addition of a methylene group to the double bond of an unsaturated fatty acid.

402   This conversion occurs as a conditional, post-synthetic modification when bacteria enter the

403   stationary phase, but also during the adaptation of bacteria in response to drastic changes in

404   the environment (Chang and Cronan, 1999). Although the exact physiological role of

405   cyclopropanized phospholipids remains unclear, it has been suggested that they improve the

406   chemical stability of the membrane, e.g. against oxidative and osmotic stress, without

407   altering the physical properties of the membrane (Grogan and Cronan, 1997; Asakura *et al.*,

408   2012). In the same perspective, the drastically increased abundance of lysophospholipids in

409   L-forms may lead to a higher membrane fluidity as well. Lysophospholipids result from the

410   Lands' cycle to remodel the composition of the fatty acids of the phospholipids by cycles of

411   deacylation and reacylation. The Land's cycle is important for the maturation of the

18

412 cytoplasmic membrane and adaptation to the environment (Shindou *et al.*, 2009).

413 Alternatively, lysophospholipids may be an intermediate product of phospholipid

414 catabolism. This process starts with β-oxidation, but the secondary degradation products are

415 not present in such an elevated amount in the L-form metabolome. Therefore, a hyperactive

416 Lands' cycle is the most plausible explanation for the abundant lysophospholipids. This

417 indicates a very active turnover to adapt membrane fluidity.

418 Although a protoplast escaping from the sacculus is apparently completely devoid of

419 peptidoglycan, we have shown here that new peptidoglycan is synthesized during L-form

420 growth and multiplication. This peptidoglycan collocates and coincides with the formation of

421 buds, although it is less delineated and more diffuse. Mostly the whole bud is covered, but in

422 many occasions only the region around the constriction site between mother and daughter

423 cell is labeled, suggesting that septal peptidoglycan synthesis is involved in bud constriction.

424 This is consistent with the finding that cefsulodin-induced *E. coli* L-forms are inhibited by

425 piperacillin that blocks PBP3, necessary for septal peptidoglycan synthesis (Joseleau-Petit *et*

426 *al.*, 2007). A functional, asymmetric Z-ring might still induce constriction assisted by septal

427 peptidoglycan synthesis to pinch off the newly formed bud. From this perspective, the

428 reproduction mechanism of this *E. coli* L-form model system is more sophisticated at the

429 molecular level compared to the *B. subtilis* model system (Leaver *et al.*, 2009), which has a

430 FtsZ-independent division mechanism.

431 Reversion of cefsulodin-induced L-forms to rods on an agar pad follows a remarkable

432 similar path as lysozyme-induced spheroplasts via a series of aberrant cells, which are often

433 filamentous, branched and thickened (Ranjit and Young, 2013). Reversion in a shaking, liquid

434 culture is more straightforward with filamentous protrusions that are pinched off eventually.

19

435   These protrusions are covered by an apparently organized layer of peptidoglycan, which may

436   even expand over the cell surface of the mother cell. This shows that removal of the inducer

437   quickly results in the activation of a functional peptidoglycan synthesis machinery to

438   produce mature peptidoglycan. The PBP profile of completely reverted cells also becomes

439   identical to rod-shaped cells. As such, the peptidoglycan synthesis machinery appears to be a

440   flexible system that produces *de novo* peptidoglycan after protoplast escape, can sustain

441   growth as a L-form spheroplast, and produce a complete new sacculus around protrusions.

442   There is an ongoing debate about the definition of L-forms. Although Joseleau-Petit

443   *et al.* (2007) originally named the cells analyzed in this study L-form-like cells, this was

444   immediately refuted by Young (2007) who considered them as L-forms. He proposed to

445   classify L-forms as class I (unstable L-forms that can revert) and class II (stable L-forms that

446   cannot revert). This suggestion was further generalized by Allan et al. (2009) who introduced

447   a unifying definition for L-forms, which he differentiated into four types: unstable and stable

448   spheroplast L-forms and unstable and stable protoplast L-forms. Where spheroplasts still

449   possess some remaining cell wall structure, protoplasts are completely devoid of any cell

450   wall. According to this definition, this work studied unstable spheroplast L-forms.

451   In conclusion, we report here an *E. coli* model system to study the L-form transition-

452   reversion cycle on a molecular basis using state-of-the-art techniques. A better

453   understanding of transient cell wall-deficiency *in vitro* will provide firmer ground to analyze

454   and interpret this phenomenon *in vivo*. Besides a contribution to the debate on the relation

455   between transient cell wall-deficiency and disease, this model also offers unique properties

456   to study *de novo* cell wall synthesis, cell wall stress response and may offer a glimpse on the

457   reproduction of more primitive bacterial life forms (Briers *et al.*, 2012a; Errington, 2013).

458 **Experimental procedures**

459 *Bacterial strains, media and growth conditions.*

460 All experiments were performed with *E. coli* K-12 MG1655 (Bachmann, 1996), except the in-

461 frame, single-gene knockout strains of the KEIO collection, which have a *E. coli* K-12

462 BW25113 background (Baba *et al.*, 2006). The tested mutants from the KEIO collection were

463 Δ*wzc*::Km^R, Δ*wcaD*:: Km^R, Δ*wcaE*:: Km^R, Δ*wcaK*:: Km^R, Δ*wcaL*:: Km^R, Δ*ugd*:: Km^R, Δ*galE*:: Km^R,

464 Δ*rcsD*:: Km^R, Δ*rcsC*:: Km^R and Δ*hrpB*::Km^R. MG1655 Δ(*argF-lac*)*U169*::*rprA142-lacZ* (kindly

465 provided by Sarah Ades, Department of Biochemistry and Molecular Biology, The

466 Pennsylvania State University, University Park, PA; Laubacher and Ades, 2008) was used to

467 measure Rcs phosphorelay activation. β-galactosidase activity was measured as described

468 previously (Zhang and Bremer, 1995). For routine growth or as reference medium, LB broth

469 was used. L-forms were grown in hypertonic medium (M broth) (3g/l beef extract (Becton,

470 Dickson and Company), 10 g/l bacteriological peptone (LabM), 5 g/l yeast extract (LabM), 5

471 g/l NaCl (Acros Organics), 0.01 M MgSO$_4$ (Acros Organics), 0.23 M sucrose (Acros Organics)),

472 supplemented with 45 μg/ml cefsulodin (Sigma-Aldrich). To induce L-forms, cells grown

473 overnight in M broth were used as inoculum. Agar plates contained 1.2 (w/v) %

474 bacteriological agar No. 1 (Lab M). For growth of the KEIO knockout strains, 50 μg/ml

475 Kanamycine was added to the medium. All growth was performed at 30°C.

476

477 *Microscopy*

478 The (fluorescent) microscopic images were acquired using two different microscopes.

479 Images from Figure 1 were obtained using a Leica TCS SPE confocal microscope (Leica

480　Microsystems GmbH, Wetzlar, Germany), operated by the Leica LAS AF interface. Sample

481　incubation temperature was controlled at 30°C, using an incubation chamber permanently

482　attached to the microscope ("The Cube", Life Imaging Services, Basel, Switzerland). An HCX

483　PL FLUOTAR 100x/1.30 oil-immersion objective was used. Transmission light images were

484　obtained using phase contrast. All other images were acquired with a temperature

485　controlled (Okolab Ottaviano, Italy) Ti-Eclipse inverted microscope (Nikon, Champigny-sur-

486　Marne, France) equipped with a TI-CT-E motorised condensor, a GFP filter (Ex 472/30, DM

487　495, Em 520/35), and a CoolSnap HQ2 FireWire CCD-camera. Operation of the microscope

488　was done using NIS-Elements (Nikon). Cells (2 µl) were dropped on agar pads in a shallow

489　depression of a microscope slide, and covered by a semi-attached cover slip. The agar pad

490　comprised either LB, hypertonic or hypertonic + cefsulodin medium with 1.2 (w/v) % agar.

491　Processing of the images was performed with the same Leica LAS AF software, Nis Elements

492　viewer, open source software ImageJ (http://rsbweb.nih.gov/ij/) and CorelDRAW X4 (Corel

493　Corporation, Ottawa, Canada) was used for final image assembly and contrast/brightness

494　adjustments.

495

496　　*Transposon mutagenesis*

497　　　A transposon knockout library of *E. coli* MG1655 was constructed using λNK1324,

498　which carries a mini-Tn*10* transposon with a chloramphenicol resistance gene, according to

499　the protocol described by Kleckner *et al.* (1991). To confirm random insertion, the library

500　was screened for auxotrophy on M9 minimal medium with 0.5% glucose. Eight out of 600

501　random clones (1.13%) did not grow, corresponding to the theoretical frequency of 1 %.

502　Overnight grown mutants in LB were replica-plated with a 96-well pin replicator on M and

22

503   MCef45 agar plates. The plates were then incubated overnight at 30°C. Mutants that were

504   able to grow on M agar but not in the L-form state on MCef45 agar plates, were after a

505   double confirmation selected for determination of the transposon inserting site using the

506   method described by Kwon and Ricke (2000).

507

508   *2D-PAGE and mass spectrometry*

509   2D-PAGE, in gel-trypsinization of selected spots and mass spectrometric analysis was

510   performed as described by Lecoutere *et al.* (2012). Briefly, all separations in two dimensions

511   were carried out using GE Healthcare devices and reagents and according to the

512   manufacturer's instructions. Iso Electric Focusing (IEF) was performed using IPG strips (24 cm

513   Immobiline DryStrips with linear pH gradient range 4-7). IEF was run in an Ettan IPGphorII.

514   Subsequently, the second dimension was run in 1 mm thick vertical gels (15%

515   polyacrylamide) using an Ettan DALT*six*. Protein spots were visualized by colloidal Coomassie

516   Brillant Blue G-250 overnight staining. Image acquisition was performed using a calibrated

517   flatbed ImageScanner, combined with LabScan software. 2-DE maps were analyzed and spot

518   data generated using ImageMaster 2D Platinum software. Selected Coomassie blue spots

519   were excised using wide-bore tips and destained. The proteins were reduced and alkylated,

520   whereafter the gel slices were sequentially hydrated, dehydrated and dried. Trypsin Gold

521   (Promega, Madison, WI; final concentration of 12.5 µg/ml) was added, followed by overnight

522   digestion. Finally, peptides were extracted from the gel by sonication. Prior to mass

523   spectrometric analysis, peptide samples were dried in a vacuum centrifuge and desalted

524   using ZipTip C_{18} pipette tips (Millipore, Bedford, MA). Peptides were separated by LC with a

525   linear 5-60 (v/v) % ACN gradient and subsequently identified by ESI-MS/MS (LCQ Classic,

23

526   ThermoFinnigan) in an *m/z* range of 300–1500. All MS data were analyzed using Sequest v.

527   1.2 within Proteome Discoverer v.1.2 (ThermoFinnigan) and Mascot v. 2.4 (Matrix Sciences)

528   against the *E. coli* MG1655 genome (NC_000913.2; 4.408 protein entries). Results from both

529   search engines were evaluated using Scaffold v. 3.6 at a minimal peptide and protein

530   probability threshold of 95% and 99%, respectively.

531

532   *Metabolite profiling and analysis*

533   Bacteria grown to mid-exponential growth phase (OD_{600nm}= 0.6; 0.45 and 0.35 for

534   cells grown in LB, M and MCef45, respectively) were sampled for metabolite profiling by fast

535   filtration as previously described (Link *et al.*, 2012). Briefly, a culture volume corresponding

536   to a biomass of 2 mL culture at OD600 = 1.0 was vacuum-filtered through a 0.45 μm pore

537   size nitrocellulose filter (Millipore, Billerica, MA, USA) and washed with 2 mL

538   ammoniumcarbonate solution (75 mM, pH 7.0). The filters were incubated in 3 mL ethanol

539   (60%) at 78°C for two minutes and the samples were snap-frozen in liquid nitrogen to be

540   stored at -80°C until further processing. Metabolite extracts were dried under vacuum at

541   30°C and resuspended in 100 μL water. Metabolites were profiled using negative mode flow

542   injection-time-of-flight mass spectrometry (Agilent 6520) and detected ions were annotated

543   based on accurate mass measurements using the strategy previously reported (Fuhrer *et al.*,

544   2011). In brief, the mass of detected anions was compared to the list of calculated masses of

545   reference metabolites compiled from the genome-scale metabolic model of *E. coli* (Feist *et*

546   *al.*, 2007) after manual curation. A mass tolerance of 1 mDa was allowed and only the best

547   hit within this tolerance was accepted. Furthermore, analysis of frequent mass shifts was

548   performed to eliminate annotations based on neutral losses and ion adducts. Metabolite

24

549 levels were relatively quantified by integration of the ion intensity signal, which was

550 previously shown to be a good approximation for the metabolite concentration (0.1 to 50

551 μM tested) in a complex biological matrix (Fuhrer et al., 2011). Statistical analysis and

552 principal component analysis was performed using Matlab R2010b (Mathworks, Natick, MA,

553 United States). Good symmetry of the volcano plots of pairwise comparisons (t-test) of all

554 detected ions confirmed that there are no relevant differences in the sampled biomass

555 (Figure S4).

556

557 *Fixation, permeabilization and staining with PBD-KZ-GFP*

558 L-forms in the mid-logarithmic phase (OD_{600nm} = 0.35), cells undergoing transition or

559 reversion were fixated during 1.5 hours at room temperature in freshly prepared 4 (v/v) %

560 formaldehyde (Sigma-Aldrich) either dissolved in hypertonic broth without (reverting cells)

561 or with 45 μg/ml cefsulodin (cells in transition or growing L-forms). After fixation, cells were

562 washed with the corresponding medium. Subsequently, cells were permeabilized for 30

563 minutes with a mixture of 1 (v/v) % Triton X-100 (Acros Organics), 50 mM EDTA (Acros

564 Organics) and 0.1% SDS (Sigma-Aldrich) dissolved in PBS. Cells were washed and incubated

565 for 15 minutes using an excess of CWB-KZ-GFP. PBD-KZ-GFP was produced and purified as

566 described in Briers *et al.* (2007). Unbound PBD-KZ-GFP was removed by washing. Samples

567 were visualized as described above.

568

569 *Determination of PBP profile*

570   Rods grown in M broth and L-forms grown in MCef45 broth were harvested in the

571   stationary phase (OD600nm=~0.9 and ~0.6, respectively). The transition and reversion

572   samples had about a 1:1 rods/L-forms ratio. Their optical densities corresponded to ~0.6 and

573   ~0.9, respectively. Cells were spun down at 16.000g for 1 min and membrane extracts were

574   prepared thereof. Thirty micrograms of membrane protein in 15 µl phosphate buffer (50

575   mM pH 7.0) was labelled at 37 °C for 30 min with a final concentration of 5 µM of Bocillin-FL

576   (Molecular Probes) and separated on a 7 % acrylamide, 3.3 % cross-linkage gel SDS-PAGE.

577   When appropriate, samples were incubated at 37 °C with clavulanic acid at a final

578   concentration of 10 µg ml^{-1} or EDTA at a final concentration of 10 mM for 30 min before

579   labelling, so as to avoid degradation of the fluorescent penicillin by β-lactamases. The PBPs

580   were visualized directly on the gel by fluorescence using Typhon9410 (Amersham

581   Biosciences) with an excitation wavelength of 588 nm and emission filter 520BP40. These

582   assays were repeated three-fold.

583

588

589

590

591   **References**

592   Allan, E.J., Hoischen, C., and Gumpert J. (2009) Bacterial L-forms. Adv Appl Microbiol

593   68:1-39.

594   Asakura, H., Ekawa, T., Sugimoto, N., Momose, Y., Kawamoto, K., Makino, S., *et al.*.

595   (2012) Membrane topology of *Salmonella* invasion protein SipB confers osmotolerance.

596   Biochem Biophys Res Comm 426:654-658.

597   Baba, T., Ara, T., Hasegawa, M., Takai, Y., Okumura, Y., Baba, *et al.* (2006)

598   Construction of *Escherichia coli* K-12 in-frame, single-gene knockout mutants: the KEIO

599   collection. Mol Syst Biol 2:2006.0008.

600   Bachmann, B. J. (1996) Derivations and genotypes of some mutant derivatives of

601   Escherichia coli K-12, p. 2460-2488. In *Escherichia coli* and *Salmonella*: cellular and molecular

602   biology. Neidhardt, F.C., Curtiss III, R., Ingraham, J.L., Lin., E.C.C., Low, K.B., Magasanik, B., *et

603   al.* (eds.) Washington DC, USA: ASM Press.

604   Bendezú, F.O., de Boer, P.A. (2008) Conditional lethality, division defects, membrane

605   involution, and endocytosis in *mre* an *mrd* shape mutants of *Escherichia coli*. J Bacteriol

606   190:1792-1811.

607   Bertsche, U., Kast, T., Wolf, B., Fraipont, C., Aarsman, M.E.G., Kannenberg, *et al.*

608   (2006) Interaction between two murein (peptidoglycan) synthases PBP3 and PBP1B in

609   *Escherichia coli*. Mol Microbiol 61:675-690.

610   Briers, Y., Volckaert, G., Cornelissen, A., Lagaert, S., Michiels, C.W., Hertveldt, K., and

611   Lavigne, R. (2007) Muralytic activity and modular structure of the endolysins of

612   *Pseudomonas aeruginosa* bacteriophages phiKZ and EL. Mol Microbiol 65:1334-1344.

613   Briers, Y., Walde, P., Schuppler, M., and Loessner, M.J. (2012) How did bacterial

614   ancestors reproduce? Lessons from L-form cells and giant lipid vesicles: multiplication

615   similarities between lipid vesicles and L-form bacteria. Bioessays 34:1078-1084.

616   Briers, Y., Staubli, T., Schmid, M.C., Wagner, M., Schuppler, M., and Loessner, M.J.

617   (2012b) Intracellular vesicles as reproduction elements in cell wall-deficient L-form bacteria.

618   PLoS One 7:e38514.

619   Callewaert, L., Vanoirbeek, K.G., Lurquin, I., Michiels, C.W., and Aertsen, A. (2009)

620   The Rcs two-component system regulates expression of lysozyme inhibitors and is induced

621   by exposure to lysozyme. J Bacteriol 19:1979-1981.

622   Chang, Y.-Y., and Cronan, J.E. (1999) Membrane cyclopropane fatty acid content is a

623   major factor in acid resistance of *Escherichia coli*. Mol Microbiol 33:249-259.

624   Dell'Era, S., Buchrieser, C., Couvé, E., Schnell, B., Briers, Y., Schuppler, M., and

625   Loessner, M. (2009). *Listeria monocytogenes* L-forms respond to cell wall deficiency by

626   modifying gene expression and the mode of division. Mol Microbiol 73:306-322.

627   Dienes, L., and Weinberger, H.J. (1951) The L-forms of bacteria. Bacteriol Rev 15:245-

628   288.

629   Domingue, G.J. (ed.) (1982) Cell wall-deficient bacteria: basic principles and clinical

630   significance. Reading, USA: Addison Wesley Publishing Co.

631   Domingue, G.J., and Woody, H.B. (1997) Bacterial persistence and expression of

632   disease. Clin Microbiol Rev 10:320-344.

633   Domínguez-Cuevas, P., Mercier, R., Leaver, M., Kawai, Y., and Errington, J. (2012) The

634   rod to L-form transition of *Bacillu subtilis* is limited by a requirement for the protoplast to

635   escape from the cell wall sacculus. Mol Microbiol 85:52-66.

636   Errington, J. (2003) Regulation of endospore formation in *Bacillus subtilis.* Nature Rev

637   Microb 1:117-126.

638   Errington, J. (2013) L-form bacteria, cell walls and the origins of life. Open Biol

639   3:120143

640   Feist, A.M., Henry, C.S., Reeed, J.L., Krummenacker, M., Joyce, A.R., Karp, P.D., *et al.*

641   (2007). A genome-scale metabolic reconstruction for Escherichia coli K-12 MG1655 that

642   accounts for 1260 ORFs and thermodynamic information. Mol Syst Biol 3:121.

643   Fuhrer, T., Heer, D., Begemann, B., and Zamboni, N. (2011) High-throughput, accurate

644   mass metabolome profiling of cellular extracts by flow injection-time-of-flight mass

645   spectrometry. Anal Chem 83:7074-7080.

646   Glover, W.A., Yang, Y., and Zhang Y. (2009) Insights into the molecular basis of L-form

647   formation and survival in *Escherichia coli*. PLoS One 4:e7316.

648   Grogan, D.W., and Cronan, J.E. (1997) Cyclopropane ring formation in membrane

649   lipids of bacteria. Microbiol Mol Biol Rev 61:429-441.

650   Hesek, D., Suvorov, M., Morio, K., Lee, M., Brown, S., Vakulenko, S.B. and Mobashery,

651 S. (2004) Synthetic peptidoglycan substrates for penicillin-binding protein 5 of Gram-

652 negative bacteria. J Org Chem 69:778-784.

653   Joseleau-Petit, D., Liebart, J.C., Ayala, J.A., and D'Ari, R. (2007) Unstable *Escherichia*

654 *coli* L-forms revisited: growth requires peptidoglycan synthesis. J Bacteriol 189:6512-6520

655   Kawai, Y., Mercier, R., and Errington, J. (2014) Bacterial cell morphogenesis does not

656 require a preexisting template structure. Curr Biol 24: 863-867.

657   Kester, J.C., and Fortune, S., M. (2014) Persisters and beyond: Mechanisms of

658 phenotypic drug resistance and drug tolerance in bacteria. *Crit Rev Biochem Mol* 49:91-101

659   Kleckner, N., Bender, J., and Gottesman, S. (1991) Uses of transposons with emphasis

660 on Tn*10*. Methods Enzymol 204:139-180.

661   Kwon, Y.M., and Ricke, S.C. (2000) Efficient amplification of multiple transposon

662 flanking sequences. J Microbiol Methods 41:195-199.

663   Lantos, P.M., Auwaerter, P.G., and Wormser, G.P. (2014) A systematic review of

664 *Borrelia burgdorferi* morphological variants does not support a role in chronic Lyme disease.

665 Clin Infect Dis 58:663-671.

666   Laubacher, M. E., and Ades, S.E. (2008) The Rcs phosphorelay is a cell envelope stress

667 response activated by peptidoglycan stress and contributes to intrinsic antibiotic resistance.

668 J Bacteriol 190:2065–2074.

669   Leaver, M., Domínguez-Cuevas, P., Coxhead, J.M., Daniel, R.A., and Errington, J.

670 (2009) Life without a wall or division machine in *Bacillus subtilis*. Nature 457:849-853.

671   Lecoutere, E., Verleyen, P., Haenen, S., Vandersteegen, K., Noben, J.P., Robben, J.,

672   Schoofs, L., Ceyssens, P.J., Volckaert, G., and Lavigne, R. (2012) A theoretical and

673   experimental proteome map of *Pseudomonas aeruginosa* PAO1. Microbiology open 1:169-

674   181.

675   Lewis, K. (2010) Persister cells. Annu Rev *Microbiol.* 64:357-72

676   Majdalani, N., Hernandez, D., and Gottesman, S. (2002) Regulation and mode of

677   action of the second small RNA activator of RpoS translation, RprA. Mol Microbiol 46:813-

678   826.

679   Markiewicz, Z., Broome-Smith, J.K., Schwarz, U., and Spratt, B.G. (1982) Spherical *E.*

680   *coli* due to elevated levels of D-alanine carboxypeptidase. Nature 297:702-704.

681   Mattman, L.H. (2001) Cell wall deficient forms – Stealth pathogens, 3 edn. Boca

682   Raton, USA: CRC Press.

683   Mercier, R., Domínguez-Cuevas, P., and Errington, J. (2012) Crucial role for membrane

684   fluidity in proliferation of primitive cells. Cell Rep 1:417-423.

685   Mercier, R., Kawai, Y., and Errington, J. (2013) Excess membrane synthesis drives a

686   primitive mode of cell proliferation. Cell 152:997-1007.

687   Onwuamaegbu, M.E., Belcher, R.A., and Soare, C. (2005) Cell wall-deficient bacteria

688   as a cause of infections: a review of the clinical significance. J Int Med Res 33:1-20

689   Mearls, E.B., Izquierdo, J.A., and Lynd, L.R. (2012) Formation and characterization of

690   non-growth states in *Clostridium thermocellum*: spores and L-forms. BMC Microbiol 12:180

691   Mercier, R., Kawai, Y., and Errington, J. (2013) Excess membrane synthesis drives a

692   primitive mode of cell proliferation. Cell 152:997-1007

693   Putri, S.P., Nakayama, Y., Matsuda, F., Uchikata, F., Kobayashi, S., Matsubara, A., and

694   Fukusaki, E. (2013) Current metabolomics: practical applications. J Biosci Bioeng 115:579-589

695   Perly, B., Smith, I.C.P., and Jarrell, H.C. (1985) Effects of the replacement of a double

696   bond by a cyclopropane ring in phosphatidylethanolamines: a ^{2}H NMR study of phase

697   transitions and molecular organization. Biochemistry 24:1055-1063.

698   Ranjit, D.K., and Young, K.D. (2013) The Rcs stress response and accessory envelope

699   proteins are required for *de novo* generation of cell shape in *Escherichia coli*. J Bacteriol

700   195:2452-2462.

701   Schnell, B., Staubli, T., Harris, N.L., Rogler, G., Kopf, M., Loessner, M.J., and Schuppler,

702   M. (2014) Cell-wall deficient *L. monocytogenes* L-forms feature abrogated pathogenicity.

703   Front Cell Infect Microbiol 4:60.

704   Shindou, H., Hishikawa, D., Harayama, T., Yuki, K., and Shimizu, T. (2009) Recent

705   progress on acyl CoA: lysophospholipid acyltransferase research. J Lipid Res 50:S46-51.

706   Smirnova, G.V., and Oktyabrsky, O.N. (2005) Glutathione in bacteria. Biochem (Mosc)

707   70:1199-1211

708   Templin, M.F., Ursinus, A., and Höltje, J.V. (1999) A defect in cell wall recycling

709   triggers autolysis during the stationary growth phase of *Escherichia coli*. EMBO J 18:4108-

710   4117

711   Tweeddale, H., Notley-McRobb, L., and Ferenci, T. (1998) Effect of slow growth on

712   metabolism of *Escherichia coli*, as revealed by global metabolite poll ("metabolome")

713   analysis. J Bacteriol 180:5109-5116

714

715   Young, K.D. (2007) Reforming L Forms: they need part of a wall after all? J Bacteriol

716   18:6509-6511

717   Zhang, X., and Bremer, H. (1995) Control of the *Escherichia coli rrnB* P1 promoter

718   strength by ppGpp. J Biol Chem 270:11181-11189.

719   Zhao, G., Meier, T.I, Kahl, S.D., Gee, K.R., and Balszczak, L.C. (1999) BOCILLIN FL, a

720   sensitive and commercially available reagent for detection of penicillin-binding proteins.

721   Antimicrob Agents Chemother 43:1124-1128

722

723

724

725

726

33

727

Figure 1: Model system of transient cell wall-deficiency.

Exemplary time-lapse series are shown for the transition from rods to L-forms (upper), multiplication of L-forms (middle), and the reversion from L-forms to rods (lower). Time points (min) and scale bar (7.5 µm) are indicated. Transitions mostly take place at the septum, but also along the lateral wall or at the poles. Spherical cell wall-deficient cells then multiply by symmetrical and asymmetrical budding, and the formation of protrusions. Upon cefsulodin removal, cells revert to a more rod-like shape (white arrow heads), they elongate and eventually get normal dimensions.

Transition
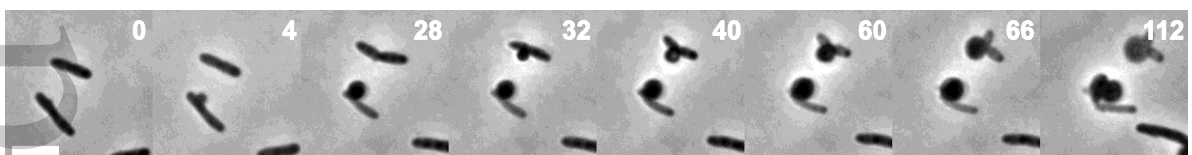
Growth
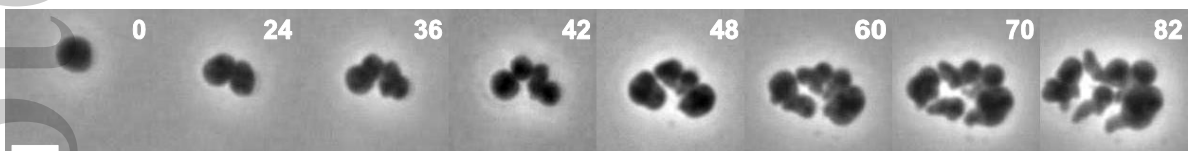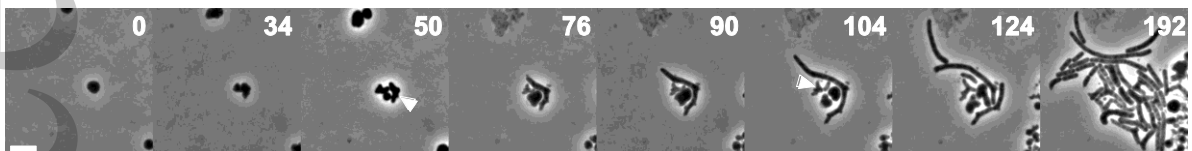
Reversion

737

738

739

740 **Figure 2: Transition and reversion rate**

741 The transition rate (A) and reversion rate (B) of cefsulodin-induced *E. coli* L-forms has been

742 quantified in liquid culture. Subpopulation of rods (black), L-forms (white) and intermediate

743 forms (grey) have been counted. Intermediate forms during transition (exposure to

744 cefsulodin) are cells that did not complete transition entirely and appear as protoplasts

745 attached to a remaining sacculus (A). During reversion (removal of cefsulodin) intermediate

746 forms represent these cells that started reversion by the formation of long protrusions, but

747 don't have a rod shape yet (B). Time starts after addition (A) or removal (B) of cefsulodin and

748 quantification takes place every 30 minutes up to 300 minutes. In every condition, between

749 50 and 300 cells were classified. Each bar represents the mean of three independent

750 experiments.

751

752

A
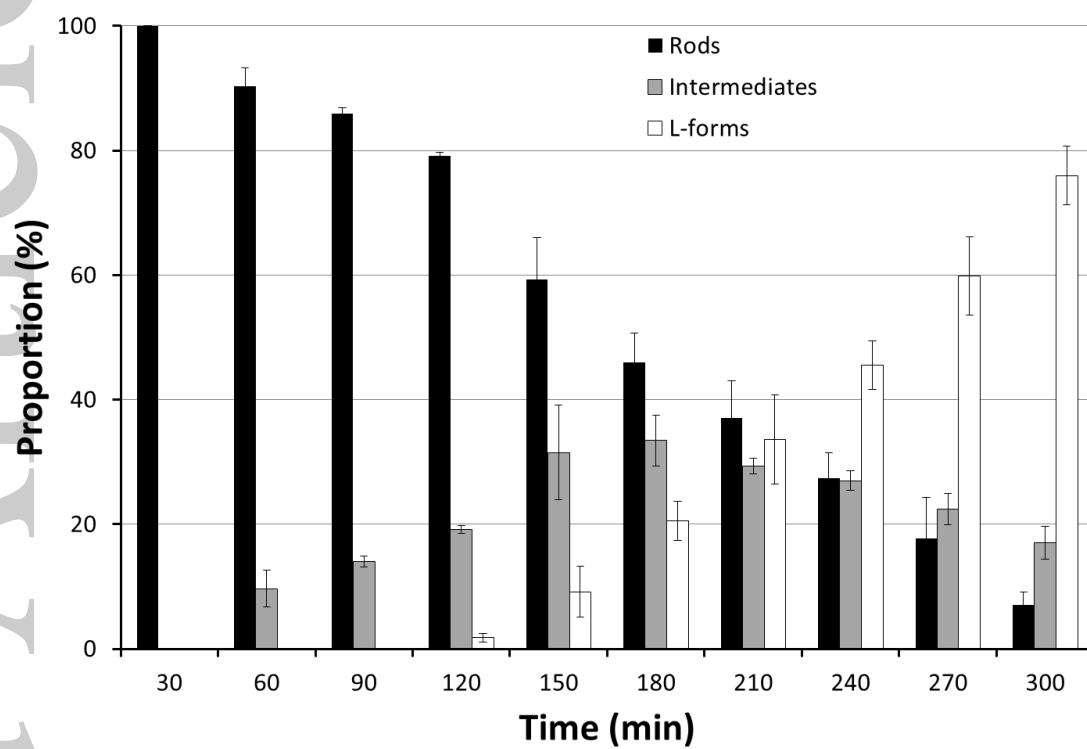
753

754

755

756

757

758

759

760

761

B

762

763

764
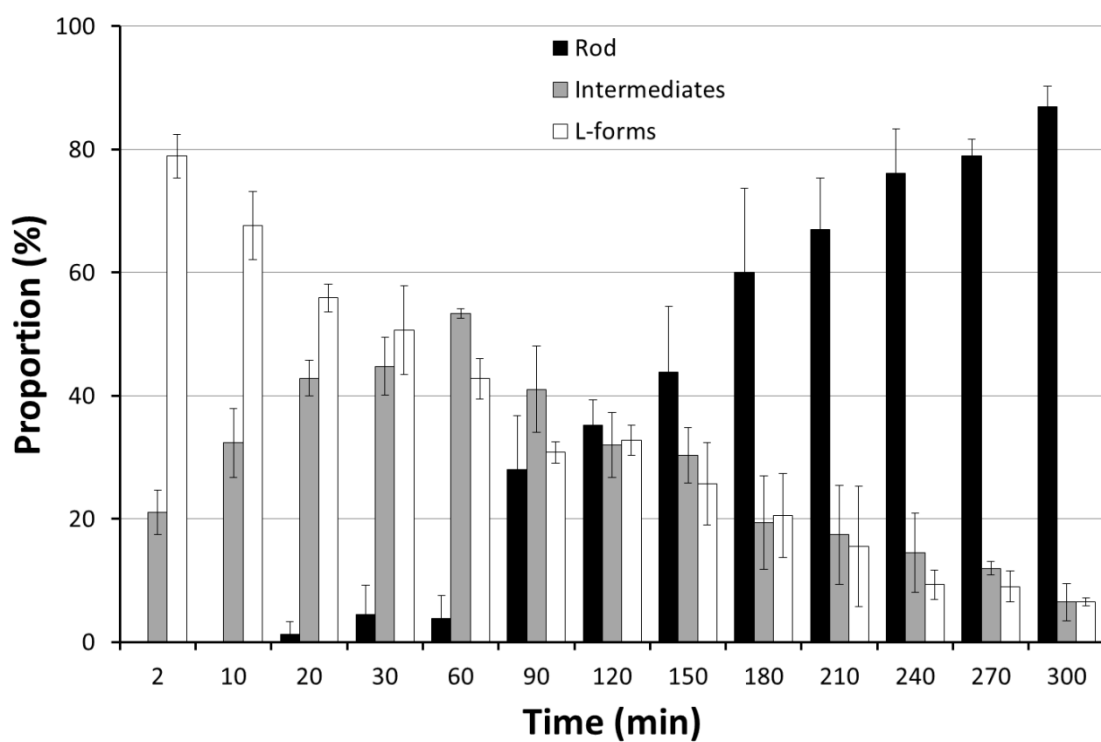
Figure 3: Overview proteome comparison between rods and L-forms.

766   A majority of spots (n=355 or 84.7% of the panproteome) is present under three conditions

767   tested. The proteome of L-forms does not reveal unique spots (n=0 or 0%) and shares more

768   spots with the proteome of cells grown in reference LB medium (n=386 or 92.1%) than with

769   the proteome of cells grown under the same hypertonic conditions in absence of cefsulodin

770   (n=356 or 84.9%).

771
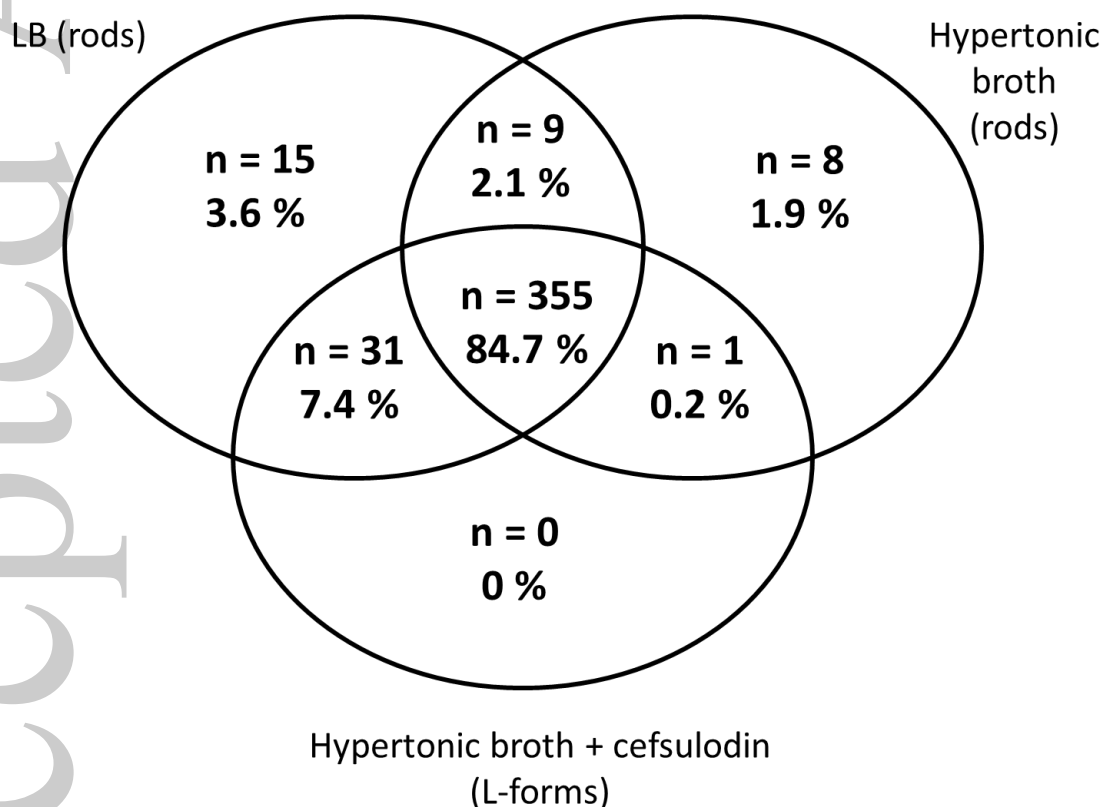
772

773

774

775 **Figure 4: Volcano plots of (lyso)phospholipids**

776 A pairwise comparison of the abundance of fourteen detected phospholipids (circles) and

777 eleven detected lysophospholipids (triangles) between L-forms (MCef45) and rods (LB) is

778 given (see also Table S2). The $\log_2$ of the fold changes are plotted (X-axis) versus the $-\log_{10}$ of

779 the corresponding P-value (Y-axis). Most extremely different metabolites of both groups are

780 annotated.
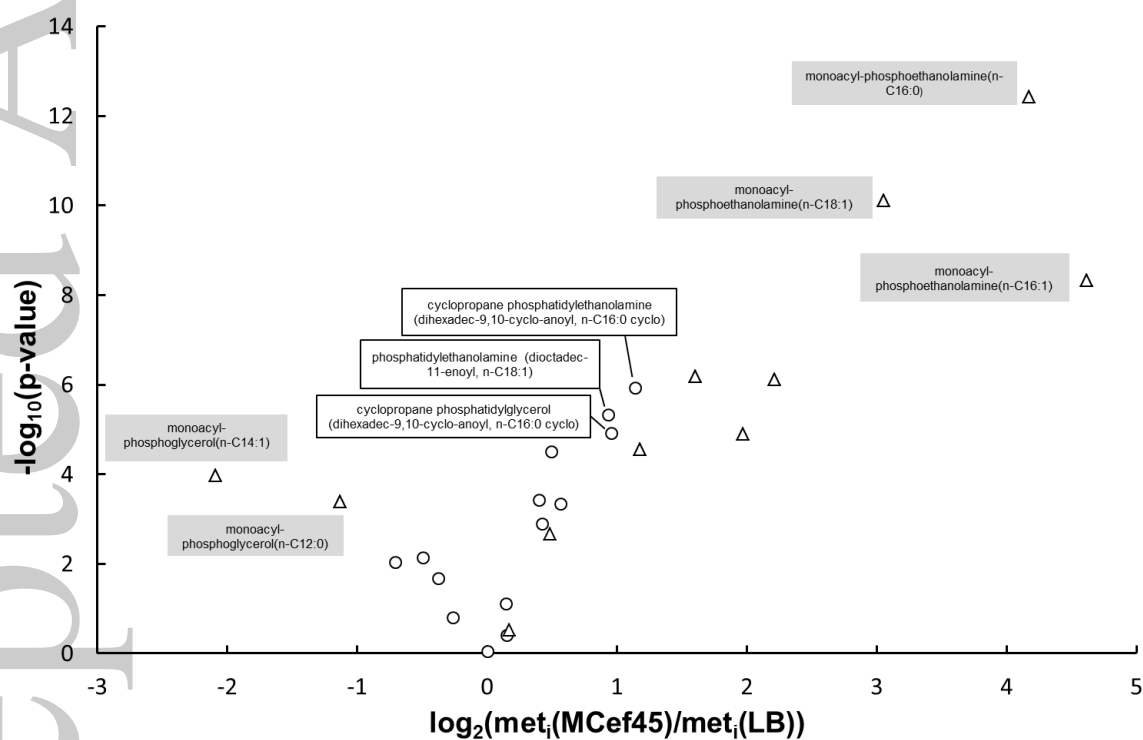
781

782

783

784

785

786

787 **Figure 5: Peptidoglycan labeling with recombinant PBD-KZ-GFP**

788 Rods undergoing transition (left), growing L-forms (middle) and reverting L-forms (right)

789 were fixated and permeabilized prior to incubation with PBD-KZ-GFP. Unbound fluorescent

790 protein was removed. The phase contrast and fluorescence channel are shown. Arrows

791 indicate colocation of peptidoglycan and the bud constriction site during L-form growth.

792 Intensities of the middle panel have been increased for clarity. Scale bar is 2 μm.

793

794

795

796　**Tables**
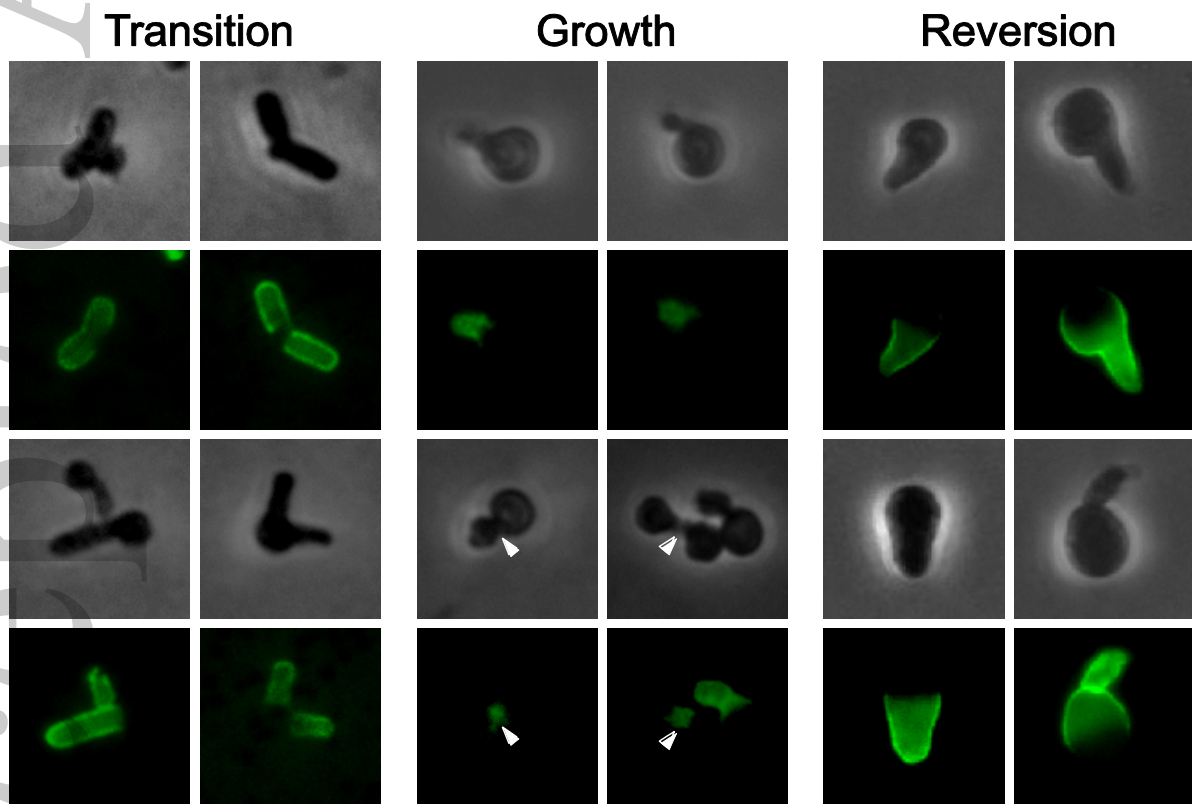
797　**Table 1: Transposon mutagenesis and identification of genes essential for L-form growth.**

798　Fourteen confirmed transposon mutants are distributed over nine different genes. The number of hits per gene is indicated. Their

799　corresponding accession number and function is given. The different genes can be subdivided in genes involved in colanic acid biosynthesis,

800　synthesis of colanic acid precursors and the Rcs two-component sensor system that activates colanic acid synthesis.

	Gene	Hits	Accession N°	Function	Group
1	*wcaD*	2	EG13572	Colanic acid polymerase	Biosynthesis
2	*wcaE*	1	EG13573	Putative colanic acid biosynthesis glycosyl transferase	Biosynthesis
3	*wcaK*	2	EG13577	Putative galactokinase, colanic acid biosynthesis protein, pyruvyl transferase	Biosynthesis
4	*wcaL*	1	EG12652	Putative colanic acid biosynthesis glycosyl transferase	Biosynthesis
5	*wzc*	1	EG13568	Protein-tyrosine kinase, involved in translocation of the growing chain	Biosynthesis
6	*ugd*	1	EG13407	UDP-glucose 6-hydrogenase (converts UDP-D-glucose in UDP-D-glucuronate)	Precursor synthesis
7	*galE*	1	EG10362	UDP-galactose-4-epimerase (converts UPD-D-galactose to UDP-D-glucose or opposite)	Precursor synthesis
8	*rcsC*	2	EG10822	Hybrid sensory kinase in two-component regulatory system with RcsB	Sensor
9	*rcsD*	3	EG12385	Phosphotransfer intermediate protein in two-component regulatory system with RcsBC	Sensor

41

801 **Table 2: PBP profile during the L-form transition-growth-reversion cycle**

802 The profile of penicillin binding proteins (PBPs) was compared for rods grown in hypertonic

803 medium, rods undergoing transition to the L-form state, multiplying L-forms, and L-forms

804 reverting to rods. The fluorescence intensities were measured and normalized for

805 comparison.

806

	Hypertonic medium	Transition	L-forms	Reverted L-forms
PBP1A	10	0,5	3	10
PBP1B	10	0	0	10
PBP1C	10	4	10	10
PBP2	10	10	10	10
PBP3	10	5	10	10
PBP4	10	20	10	10
PBP5	10	10	30	10
PBP6	10	12	40	10
PBP7	10	10	10	10

807

808

809

810

811

812

813

814